

# Synthesis, characterization and evaluation of some graphene oxide derivatives and their application as corrosion inhibitors for carbon steel alloy type C1025 in hydrochloric acid

Ali A.Naser, Alaa S. Al-Mubarak and Hadi Z. Al-Sawaad

University of Basrah, College of Science, Department of Chemistry, Iraq

\*E-mail: [hadiziara@yahoo.com](mailto:hadiziara@yahoo.com)

## Abstract

In this work, graphene oxide was modified first by a reaction with sulfanilic acid and second, by a reaction with sulfamic acid. The prepared compounds were characterized by XRD, Raman shift, FESEM and EDS techniques. GO functionalized sulfanilic acid (GOC) and GO functionalized sulfamic acid (GOD) were evaluated as anticorrosion inhibitors for carbon steel alloy (C1025) in acidic 0.1 M HCl environment at 298 K by the electrochemical method (Tafel plot method). The data reveals that the efficiencies of GO, GOC and GOD are 77.4%, 90.2% and 92% respectively at optimal concentrations of 100, 50 and 70 ppm, respectively. The effect of temperature on the corrosion reaction was studied and the results show that increasing the temperature in the range of 298, 308, 318 and 328 K decreased the efficiency. Furthermore, the thermodynamic and kinetic parameters such as the activation energy ( $E_a$ ), enthalpy of activation ( $\Delta H^*$ ), Gibbs free energy of activation ( $\Delta G^*$ ) and entropy of activation ( $\Delta S^*$ ) were studied. The results indicate that the prepared inhibitors obey the Langmuir adsorption isotherm with  $R^2$  near unity. The equilibrium constant  $K_{ads}$ , Gibbs free energy of adsorption ( $\Delta G_{ads}^0$ ), enthalpy of adsorption ( $\Delta H_{ads}^0$ ) and entropy of adsorption ( $\Delta S_{ads}^0$ ) were calculated.

**Keywords:** graphene oxide, sulfanilic acid, microwave, carbon alloy.

Received: October 29, 2019. Published: November 18, 2019

doi: [10.17675/2305-6894-2019-8-4-11](https://doi.org/10.17675/2305-6894-2019-8-4-11)

## 1. Introduction

Since the discovery of graphene by Andre Geim and Konstantin Novoselov in 2004, graphene has attracted attention in several fields: it has excellent mechanical, thermal and electrical properties, high chemical stability, large specific surface area, high tensile strength and high Young's modulus due to hexagonal structure, 2D and arranged  $sp^2$  bonded carbon material network. Graphite is the raw material for graphene derivatives, such as graphene oxide (GO). GO is produced by oxidation of graphite with sonication to give GO [1–3].

GO has heavily oxygenated groups to which functional groups like carbonyl, hydroxyl, carboxylic and epoxide can be attached. Through these groups, GO allows novel compounds to be synthesized [4, 5]. This study includes the synthesis of novel compounds

from graphene oxide by microwave irradiation. The compounds produced may be used as anti-corrosion agents due to the presence of functional groups. The use of microwave irradiation in natural science has been investigated broadly in the recent decade. Microwave irradiation has a number of advantages such as: the reaction times decreased, the yields of compounds increased and work up in green chemistry is easier [6].

Corrosion is characterized as the weakening of a material, usually a metal or alloy, due to response to its conditions, which requires the nearness of a cathode, an anode, electrolyte and electrical circuit [7]. Corrosion is a major problem in industry where it causes a high upkeep cost and consumption of a metal or alloy. Corrosion of carbon steel is viewed as of considerable liability, both in economical and environmental respects, attributable to the tremendous utilizations of carbon steel by many industries. The mechanism of corrosion prevention for metals is of fundamental significance for increasing their lifespan in corrosive environments, as the corrosion of metals or alloys in acidic medium causes considerable losses [8–10].

Acid solutions are commonly used in industries for removal of undesirable scale in processes such as cleaning, pickling, and descaling. To reduce the rate of corrosion or control it for metals and alloys, inhibitors were used for the protection of metals or alloys from corrosion in acidic medium. Excellent inhibitors exist among organic compounds containing heteroatoms such as N, S and O, where the inhibition efficiency of compounds should increase in the order  $O < N < S$  [11–13]. In the present study, we have synthesized two compounds, *i.e.*, sulfanilic acid and sulfamic acid based functionalized graphene oxide (GOC and GOD) respectively, and evaluated their anti-corrosion effect in acid media for carbon steel alloy corrosion in 0.1 M HCl at different temperatures using measurements by electrochemical methods, including the Tafel plots, and also calculated the thermodynamic and kinetic functions of adsorption on the metal surface. The positive outcomes demonstrate the significance of this work.

## 2. Experimental

### 2.1. Materials

The carbon steel alloy employed in this study was C1025 type. The alloy composition is shown in Table 1 below.

The materials used in this study were different materials from different companies, including: graphite powder, hydrogen peroxide, sodium nitrate, sulphuric acid, hydrochloric acid, potassium permanganate, ethanol, sulfanilic acid, sulfamic acid and *N,N*-dimethylformamide (DMF).

**Table 1.** Carbon steel composition (C1025).

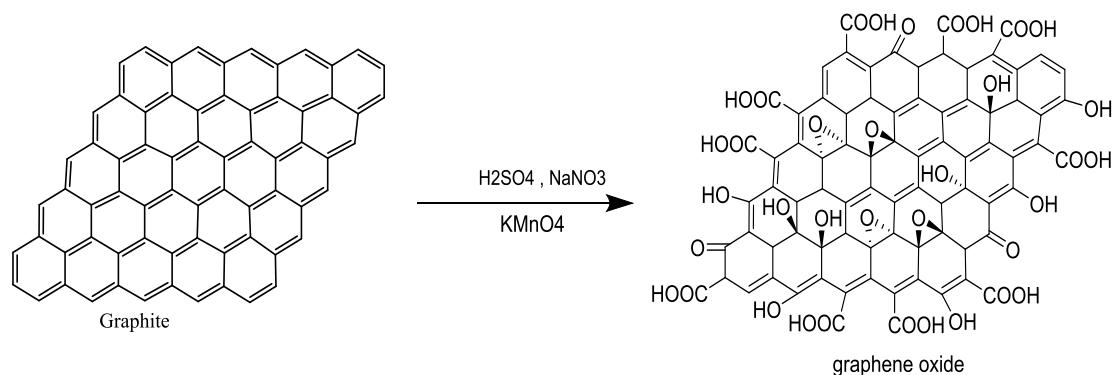
Alloy	Composition % w/w										
	C	S	P	Mn	Si	Cr	Ni	Cu	As	other	Fe
Carbon steel (C1025)	0.27	0.002	0.003	0.69	0.2	0.029	0.008	0.038	0.15	0.1249	Balance

## 2.2. Synthesis of GO

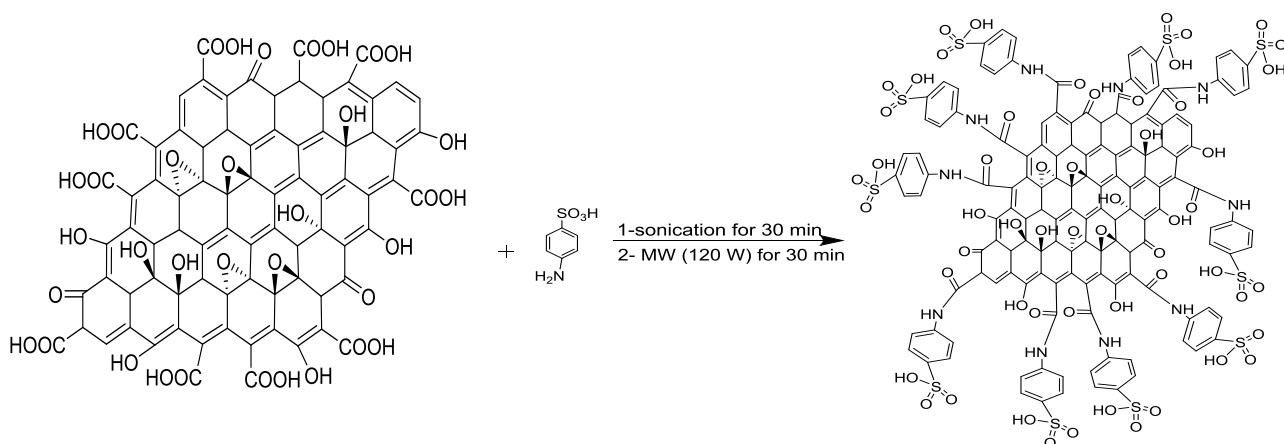
Graphene oxide was synthesized using the modified Hummer's method. In a round bottom flask, 1 g of graphite powder, 0.5 g of sodium nitrate and 23 mL of  $H_2SO_4$  were mixed together with stirring for 30 min in an ice bath. After that, 3 g of  $KMnO_4$  was added very slowly to the suspension over a period of 3 h. After it was finished, an amount of hydrogen peroxide was added to the mixture until the reaction ceased. The mixture was dried and exfoliated by sonication to get the GO solids that were repeatedly washed with 5% HCl and DI  $H_2O$ . After that, the product was dried in a furnace at a temperature of 70–80°C for 4 h to obtain graphene oxide [14–16].

## 2.3. Synthesis of GOC and GOD compounds

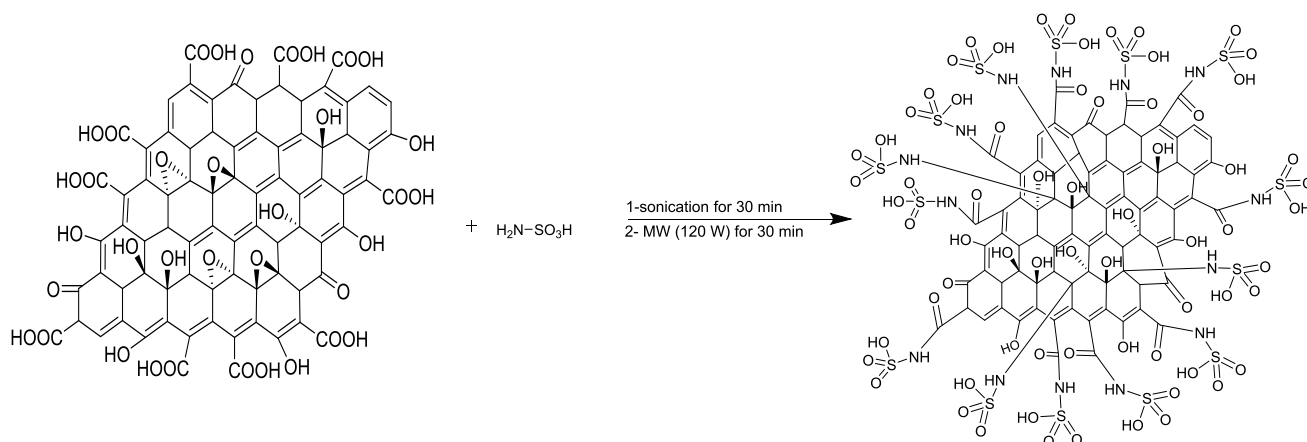
Graphene oxide was functionalized with sulfanilic acid (GOC) and sulfamic acid (GOD) using a microwave, where the two products were obtained by the same procedure by just different molecular weight to prepare GOC. 0.5 g of GO was dispersed in 50 ml DMF by using ultra sonication for 30 min in a beaker, afterward 1.73 g and 10 mmole of sulfanilic acid was added to the mixture and also dispersed by ultra sonication for 30 min. The suspension was heated in a microwave for 30 min, 20% power (140 W). After that, the suspension was washed several times with 300 ml anhydrous ethanol, then washed several times with distilled water and ethanol. The GOC thus obtained was dried at 70°C for 6 h to collect the black powder product (GOC). The synthesis of GOD was performed using same procedure, but with different weight of sulfamic acid (0.97 g) [17]. The general chemical reactions are shown below in Schemes 1–3.



**Scheme 1.** The general chemical reaction of GO synthesis.



**Scheme 2.** The general chemical reaction of GOC synthesis.



**Scheme 3.** The general chemical reaction of GOD synthesis.

#### 2.4. Preparation of working electrodes

Strips of carbon steel alloy (C1025) with the following dimensions were used: length 2 cm, width 2.55 cm, and thickness 0.35 cm. The total area of the strips was 12.4925 cm<sup>2</sup>. The strips were immersed in solution, then ground with increasing grades of Silicon carbide paper to different smoothness (80, 120, 200, 400, 600). Afterward they were washed with distilled water, ethanol, acetone and dried, then stored in a dry place at room temperature and placed in desiccators containing silica gel for protection from moisture.

#### 2.5. Electrochemical cells

The electrochemical cell for the corrosion test was used in the present study. The cell consists of a 100 ml vessel connected with three electrodes arranged as follows: 1 – a platinum electrode was used as the counter electrode; 2 – carbon steel specimen used as the working electrode; 3 – a saturated calomel electrode (SCE) was used as reference electrode.

## 2.6. Potentiodynamic studies (Tafel plots)

This technique is commonly employed for measuring corrosion resistance and a wide variety of functions, to measure current density *vs.* electric potential, through setting up the open circuit potential (OCP) for 20 min. The polarization curve can be acquired by scanning in the potential range between  $-2.5$  to  $+2.5$  mV (*vs.* OCP) using a computer to control a potentiostat/galvanostat at a scanning rate of  $10 \text{ mV s}^{-1}$ .

## 2.7. Preparation of solutions

The prepared compounds were individually synthesized at different concentrations (10, 30, 50, 70 and 100 ppm) at 298 K and at different temperatures (308, 318 and 328 K) for finding the optimal concentration, with 0.1 M HCl as the corrosive medium.

## 2.8. Instruments

The prepared compounds were characterized using different techniques such as Field Emission Scanning Electron Microscopy (FESEM) FEI NOVA nanosem450, Nano NOVA FE-SEM at an accelerating voltage of 15 kV with magnification range from 20X to 5000X, Energy Dispersive Spectroscopy (EDS) Bruker x Flash6i 10 performed between 0 and 20 kV, Raman shift Spectroscopy (Renishaw, England), and backscattering geometry with a CCD detector. A Nd-YAG laser 532 nm with a 50 magnification objective was used for the measurements. Laser excitation, XRD (X-ray Diffraction) spectroscopy XRD – Philips-X, at Tehran university Rigaku diffractometer using Ni-filtered Cu  $K\alpha$  radiation ( $\lambda = 0.15406 \text{ nm}$ ) operating under a current of 40 mA and a voltage of 40 kV.

# 3. Results and discussion

## 3.1. Characterization by Raman spectroscopy of prepared compounds

Raman spectroscopy is an excellent technique to characterize the structure, and carbon products and crystal structure, where the GO spectrum shows two small bands, where D band at  $1359.57 \text{ cm}^{-1}$  which indicates a band of disordered  $sp^2$  structures, while the G band at  $1602.48 \text{ cm}^{-1}$  is attributed to first order scattering for in-phase vibration of the  $E_{2g}$  phonon, also the vibration mode of carbon atoms ( $sp^2$ ), while the small band (2D) at  $2935.05 \text{ cm}^{-1}$  is attributed to dispersive bands observed in derived graphite carbon materials as shown in Figure 1 below. While GOC and GOD compounds derived from GO show two clear peaks at D and G bands, where the D bands are at  $1330.75$ ,  $1349.96 \text{ cm}^{-1}$  while the G bands are at  $1575.03$ ,  $1592 \text{ cm}^{-1}$  for GOC and GOD, respectively. Interpretation of the Raman spectrum for GO derivatives indicates that the D bands of GOC and GOD with the above wave numbers were slightly shifted to lower wave number values compared with the D band of GO. This confirms the presence of new group in the GO structure upon modification; that evidence the introduction of nitrogen atom into the carbon layers in GO. On the other hand, the intensity values of GO, GOC and GOD as

shown in Figure 1. Note there is a change in ID/IG intensity ratio due to electronic conjugation state of GO upon modification and the ID/IG intensity ratio (0.9, 1.94) for GO, GOC and GOD respectively. An increase in ID/IG intensity indicates an increase in disorder in GO lattice after modification and this indicates a decrease in the average size of the  $sp^2$  carbon atoms in GO derivatives. This confirms the suggestions for GO modification with other compounds [18–24].

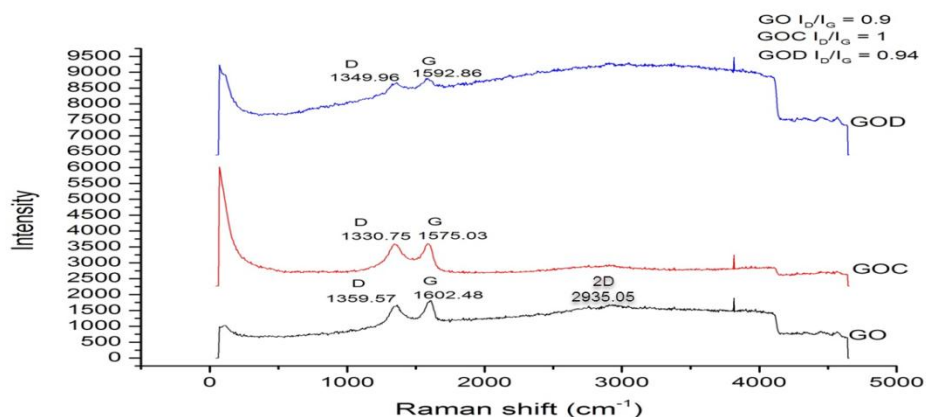


**Figure 1.** Raman spectrums for GO, GOC and GOD.

### 3.2. Morphological surface characterization by FESEM of prepared compounds

The surface morphology of the prepared compounds GO, GOC and GOD was examined by (FESEM) Field Emission Scanning Electron Microscopy technical analysis [5]. From the FESEM image one can calculate the average particle size of the synthesized compounds using the Image-J program. The FESEM images and particle sizes of compounds shown in Figure 2 and Table 2 indicate that these compounds have nanoparticle characters. The FESEM images of graphene oxide (GO) show in Figure 2 below has a smooth and flat sheet with low thickness and also has kinked areas and a lot of wrinkled edges, where the surface of GO has light gray color and consists of several layers, and also includes some cavities, crumpled flakes and stacks associated with each other [19, 25, 26]. The FESEM images of GOC and GOD are shown in Figure 2. In GOC there are multiple layers, part of which are dark gray indicating many layers, while a few layers are light colored indicating re-stacked layers. The layers are crumpled and rippled and have sharp edges. In GOD, the appearance of the layers is light gray and they have wrinkled and kinked areas. The dark gray colored layers were folded with each other. This difference of GOC and GOD from GO are indicative of sulfanilic acid and sulfamic acid grafting with the graphene oxide (GO).

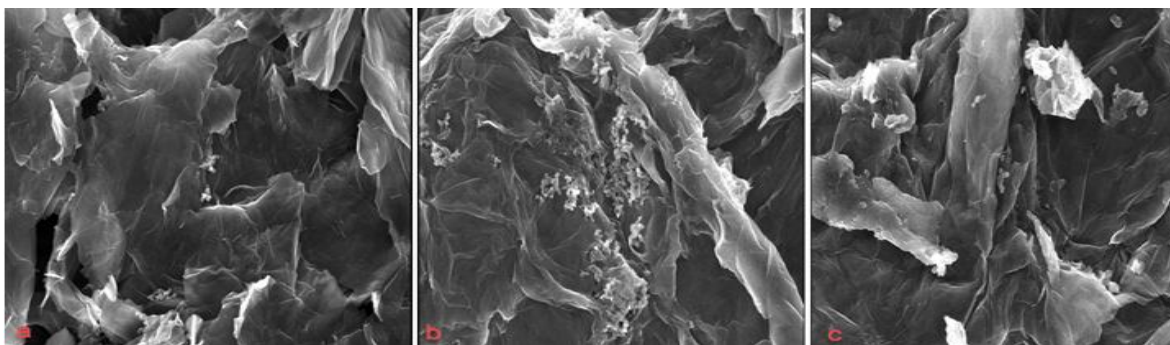


**Figure 2.** FESEM Images of prepared compounds a: GO, b: GOC and c: GOD.

**Table 2.** Average nanoparticle size in GO, GOC and GOD.

No.	Com	Particle size (nm)	Average
1	GO	52, 40, 52, 27.5, 48, 41.8	43.55
4	GOC	31, 30.2, 33.2, 26.1, 50.3	34.16
5	GOD	59.90, 52.11	56
10	GOI	177, 199.7, 145.3, 341.3	215.83

### 3.3. Analysis of elemental composition of prepared compounds by EDS

(EDX) Energy Dispersive X-ray spectroscopy analysis is performed along with FESEM. EDX was used as an analytical technique for analysis of the elemental composition and chemical characterization of compounds [24]. The spectra and EDX data analysis are shown in Figures 3–5 and Tables 3–5. The EDX spectrum of GO shown in Figure 3 reveals two peaks related to C and O at 0.277 and 0.525 keV energy, respectively, with 71.45, 28.55 weight% and 76.83, 23.17 atomic% of C and O, respectively. This indicates that GO prepared is in good agreement with the published studies on graphene oxide synthesis [26].

The EDX spectra of GOC and GOD shown in Figures 4 and 5 reveal that new peaks appear for N and S at 0.392 and 2.307 keV for GOC and GOD, respectively. This is due to amino functionalization of GO for both sulfanilic acid and sulfamic acid, which leads to grafting on the GO surface. In GOC another element was present as impurities on the surface of GOC with a new peak at 2.71 keV attributed to Cl atom, but this peak was very weak and corresponded to 0.0012(Cl) wt% and 0.01(Cl) at%. The following weight percentages were found in GOC and GOD, respectively: 58.87 wt% (C), 35.80 wt% (O), 3.25 wt% (S), 2.04 wt% (N); 60.31 wt% (C), 30.97 wt% (O), 5.11 wt% (S), 3.61 wt% (N). The atomic percentages in GOC and GOD are as follows: 66.38 at% (C), 30.28 at% (O), 1.37 at% (S), 1.96 at% (N), 68.15 at% (C), 26.20 at% (O), 2.15 at% (S), 3.5 at% (N), respectively. Loading of N and S from sulfanilic acid and sulfamic acid on GO leads to a change in the elemental composition of C and O compared with GO. This indicates that the compounds were successfully prepared in the present study.

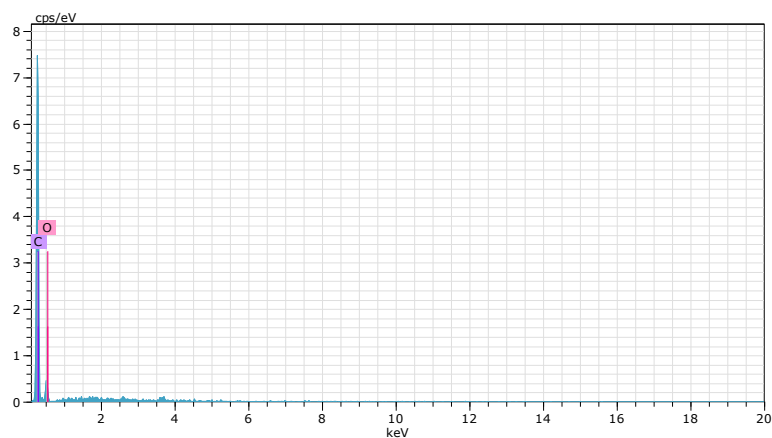


Figure 3. EDX spectra of GO.

Table 3. EDX spectra analysis for GO.

Element	AN.	Series	keV	[norm.wt. %]	[norm.at. %]
C	6	K-series	0.277	71.45	76.83
O	8	K-series	0.525	28.55	23.17
Sum:				100	100

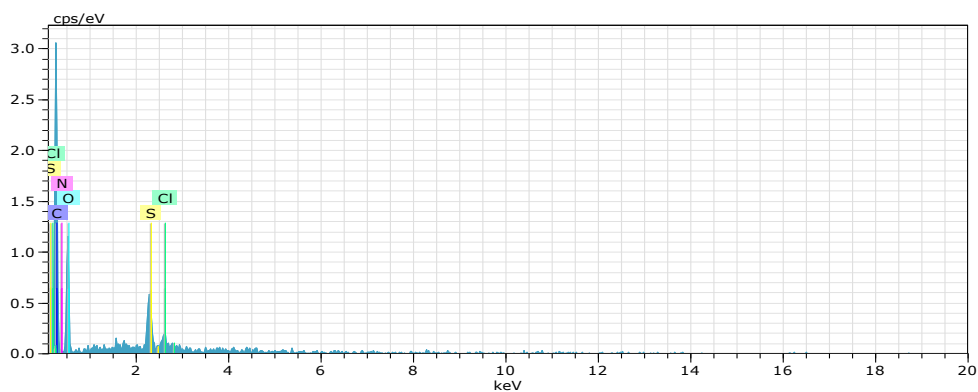
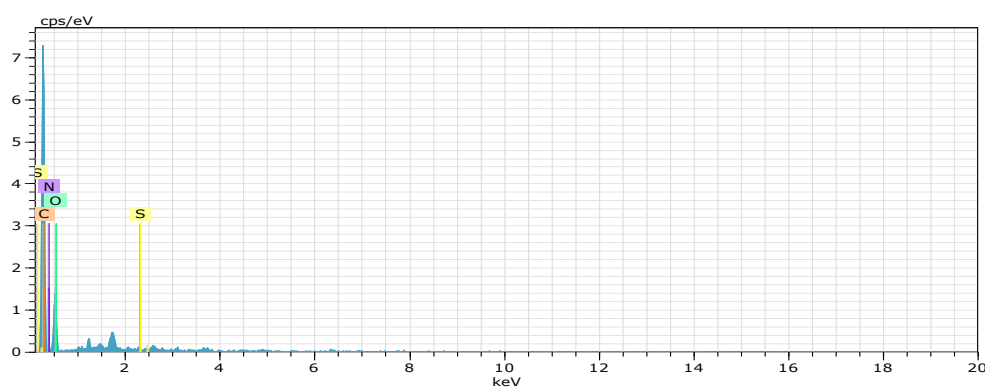


Figure 4/ EDX spectra of GOC.

Table 4. EDX spectra for GOC.

Element	AN.	Series	keV	[norm.wt. %]	[norm.at. %]
C	6	K-series	0.277	58.87	66.38
O	8	K-series	0.525	35.80	30.28
S	16	K-series	2.307	3.25	1.37
N	7	K-series	0.392	2.04	1.96
Cl	17	K-series	2.71	0.04	0.01
Sum:				100	100



**Figure 5.** EDX spectra of GOD.

**Table 5.** EDX spectra analysis for GOD.

Element	AN.	Series	keV	[norm.wt. %]	[norm.at. %]
C	6	K-series	0.277	60.31	68.15
O	8	K-series	0.525	30.97	26.20
S	16	K-series	2.307	5.11	2.15
N	7	K-series	0.392	3.61	3.5
Sum:				100	100

### 3.4. Characterization of prepared compounds by X-ray Diffraction (XRD)

X-Ray diffraction (XRD) is a broadly employed technique for characterization of crystalline materials. It is used to measure the average dispersings between the layers and to determine the orientation of grains or single crystals [22]. The XRD patterns of GO, GOC and GOD are shown in Figure 6. The pattern of GO showed a sharp peak at ( $2\theta = 11.15^\circ$ ) with  $d_{\text{spacing}} = 8 \text{ \AA}$ . This is due to the oxidation process of graphite. According to the published research, graphite has a peak at  $26.6^\circ$  with  $d_{\text{spacing}} = 3.3 \text{ \AA}$ . This means that upon oxidation, GO acquires a new peak at  $11.15^\circ$  with a decrease in the interlayer spacing [20, 23, 27]. Compared with GO, GOC and GOD will have different peak values and interlayer spacing. It was found that the peak of GOC ( $10.91^\circ$ ) was lower than that of GO ( $11.15^\circ$ ) with some increase in the interlayer spacing ( $8.1 \text{ \AA}$ ). It was also found that the GOC spectrum had many peaks due to the presence of some impurities during GOC synthesis, as shown in Figure 6. GOD showed a peak at  $13.66^\circ$  which was higher than that of GO ( $11.15^\circ$ ) with an interlayer spacing decrease ( $6.5 \text{ \AA}$ ). This indicates that the amino groups of sulfanilic acid and sulfamic acid were successfully attached to the GO surface during the modification. Generally, incorporation of amino groups does not significantly change the crystalline structure of GO [4, 20, 28, 29].

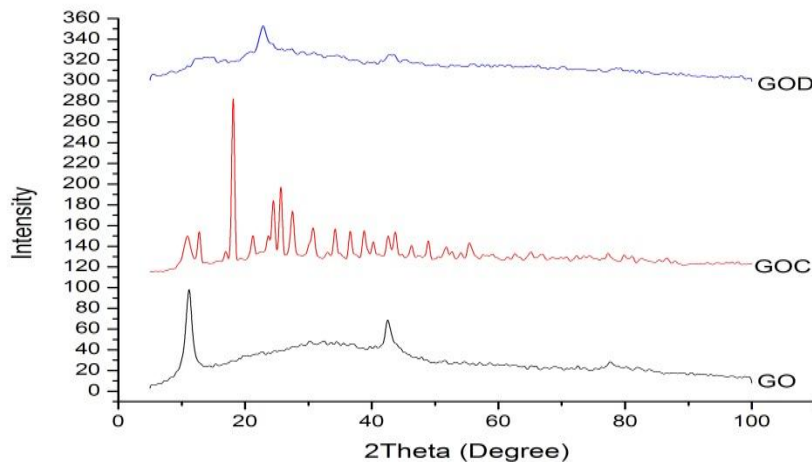


**Figure 6.** XRD spectrums of GO, GOC and GOD.

### 3.5. Polarization studies (Tafel plot)

Table 6 and Figure 7 below show the electrochemical data obtained from Tafel plots at several concentration of prepared inhibitors GO, GOC and GOD as anticorrosion agents for carbon steel alloy (C1025) in 0.1 M HCl. Generally, an increase in the concentration of the prepared inhibitors significantly changed the electrochemical factors obtained from the Tafel plots. It was noted that the corrosion current density ( $I_{\text{corr}}$ ) significantly decreased in the presence of the inhibitors compared with the non-inhibited solution, which is due to the adsorbed layer of inhibitor on the surface of the alloy.

This generates a high resistance between the surface of the alloy and the solution, which either increases or decreases  $I_{\text{corr}}$ , thus leading to changes in the corrosion rates. On the other hand, the corrosion potential ( $E_{\text{corr}}$ ) value is affected by increasing the concentration of inhibitors compared to the non-inhibited solution. Notice there is little a displacement between the  $E_{\text{corr}}$  in the presence of inhibitor and its absence, dependent on the difference between  $E_{\text{corr}}$  values in the presence and absence of an inhibitor where if  $E_{\text{corr}}$  value was greater than the ( $-85$  mV) this indicates that the inhibitor type is either anodic or cathodic, while if  $E_{\text{corr}}$  value was less than ( $-85$  mV) this implies that the inhibitor is of mixed type. In the present study the maximum displacement in  $E_{\text{corr}}$  values was 6, 45 and 48 mV for GO, GOC and GOD respectively, that means that the prepared inhibitors were of mixed type [30].

The Tafel constant values ( $\beta_a$  and  $\beta_c$ ) are shown in Table 6 and Figure 7 below. It can be noticed that the values of  $\beta_c$  varied differently in the presence of various inhibitor concentrations, which indicates changes in the mechanism of inhibition. This means that the prepared inhibitors affect the mechanism of cathodic reaction represented by the oxygen reduction and hydrogen evolution reactions. It shows that the prepared inhibitors act by simple blockage of the surface by adsorption, *i.e.*, this indicates an increase in the number of adsorbed inhibitor molecules on the alloy surface with an increase in inhibitor

concentration. The  $\beta_a$  values change with addition of inhibitors, which is attributed to that the prepared inhibitors are first adsorbed on the alloy surface and impede the passage of metal ions from the oxide-free metal surface into the solution by blocking the reaction sites on the metal surface affecting the anodic reaction mechanism. This indicates that the inhibitors prepared in this study are mixed types inhibitors [31, 32].

Furthermore, the polarization resistance ( $R_p$ ) values shown in the tables below significantly increase in the presence of an inhibitor compared to the non-inhibited solution, *i.e.*, the greater the concentration of the inhibitor, the more resistant the alloy surface. If  $R_p$  increases or decreases, the corrosion rates change. The  $R_p$  value in the absence of inhibitor was  $16.488 \Omega \cdot \text{cm}^2$ , whereas the  $R_p$  values at the optimal concentration of inhibitors were 72.96, 167.09 and 206.09 at concentrations 70, 50 and 70 ppm, respectively.

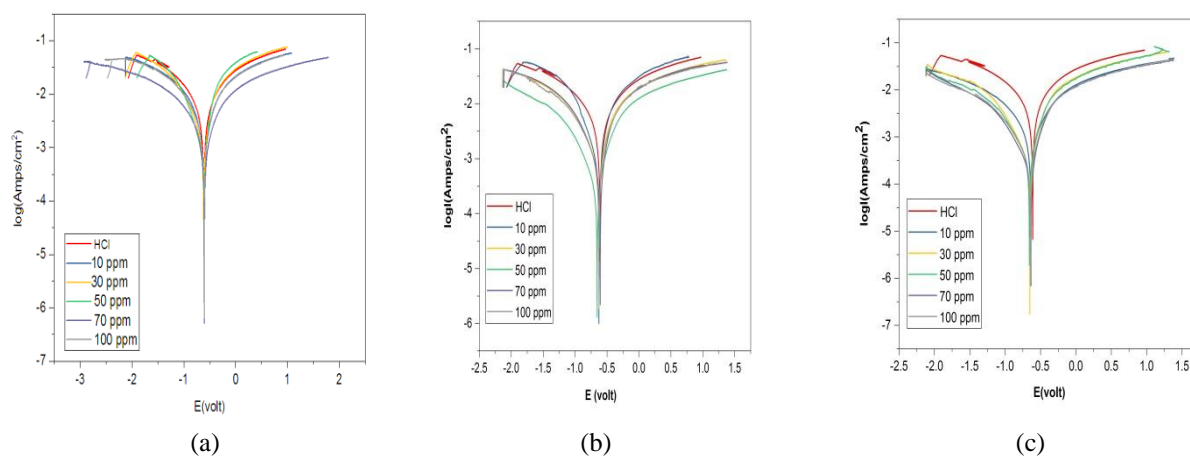
On the other hand, the corrosion rate values (CR) decrease significantly at different concentrations of prepared inhibitors compared to the non-inhibited solution. Note that the CR value in the absence of an inhibitor was high (505.54 mpy), while CR values in the presence of inhibitors at the optimal concentrations were very low, namely, 114.24, 49.887 and 40.446 at GO, GOC, and GOD concentrations of 100, 50 and 70 ppm, respectively. It follows from the above data that the CR value decreases in the presence of an inhibitor. The values of inhibition efficiency (IE%) and surface coverage ( $\theta$ ) depend on the corrosion rate. Increasing the concentration of the inhibitors increases inhibition efficiency. Note that the values of (IE%) and ( $\theta$ ) at the optimal concentration of prepared inhibitors were (77.4, 0.774), (90.2, 0.902), (92, 0.92) for GO, GOC and GOD at concentrations of 100, 50 and 70 ppm, respectively.

Table 7, Figures 8 and 9 demonstrate the effect of temperature change on the corrosion rate (CR) at the optimal concentrations of the prepared inhibitors at different temperatures (298–328 K). Both ( $I_{\text{corr}}$ ) and (CR) increase as the temperature increases, while ( $R_p$ ) and (IE%) decrease due to the effect of temperature change on the inhibition efficiency of alloy based on two principles: if the inhibition efficiency decreases with a temperature increase, this is attributed to physical adsorption, while if the inhibition efficiency increases with a temperature increase, this is attributed to chemical adsorption. The inhibitors prepared in this present study were of physical adsorption type.

The increase in the corrosion rate and the decrease both in inhibition efficiency and degree of adsorption with increasing temperature agrees with many researchers who studied corrosion, where a temperature increase led to an increase in kinetic energy of the inhibitory particles and decreased both the efficiency of adsorption and surface coverage by inhibitor molecules [33].

**Table 6.** Corrosion parameters in the absence and presence of GO, GOC and GOD inhibitors at 298 K.

Comp.	Conc. (ppm)	$E_{\text{corr}}$ (mV)	$I_{\text{corr}}$ ( $\mu\text{A}\cdot\text{cm}^{-2}$ )	CR (mpy)	$\beta_a$ mV	$\beta_c$ mV	$R_p$ ( $\Omega\cdot\text{cm}^2$ )	% IE	$\theta$
HCl	Blank	-611	1092	505.54	214.94	-240.19	16.488	–	–
	10	-605	412.1	190.82	335.45	-367.41	43.682	62.3	0.623
GO	30	-617	391.5	181.28	214.02	-394.33	45.982	64.2	0.642
	50	-605	394.2	182.52	366.64	-411.11	45.668	63.9	0.639
	70	-609	309.7	143.41	161.77	-377.31	58.124	71.7	0.717
	100	-603	246.7	114.24	443.65	-458.22	72.963	77.4	0.774
GOC	10	-628	330.8	153.17	190.85	-346.78	54.419	69.7	0.697
	30	-628	268.9	124.51	268.5	-535.06	66.947	75.4	0.754
	50	-656	107.8	49.887	255.01	-509.18	167.09	90.2	0.902
	70	-627	234.5	108.51	262.05	-450.5	76.817	78.6	0.786
	100	-608	209.2	96.848	193.33	-367.89	86.067	80.9	0.809
GOD	10	-636	216.4	100.19	439.13	-485.71	83.197	80.2	0.802
	30	-653	136.7	63.279	244.97	-870.47	131.72	87.5	0.875
	50	-659	132.4	61.298	243.95	-787.37	135.98	87.9	0.879
	70	-638	87.5	40.446	214.84	-676.57	206.09	92	0.92
	100	-642	109.8	50.83	260.14	-734.72	163.99	90	0.90

**Figure 7.** Tafel plots in the absence and presence of inhibitors. a: GO, b: GOC and c: GOD at 298 K.

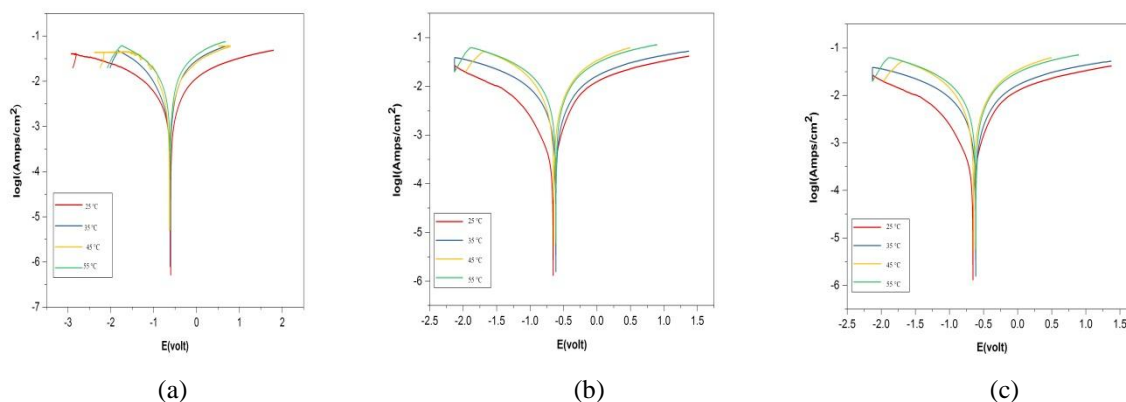


**Figure 8.** Tafel plots in the presence of GO, GOC and GOD inhibitors at optimal concentrations and at different temperatures.

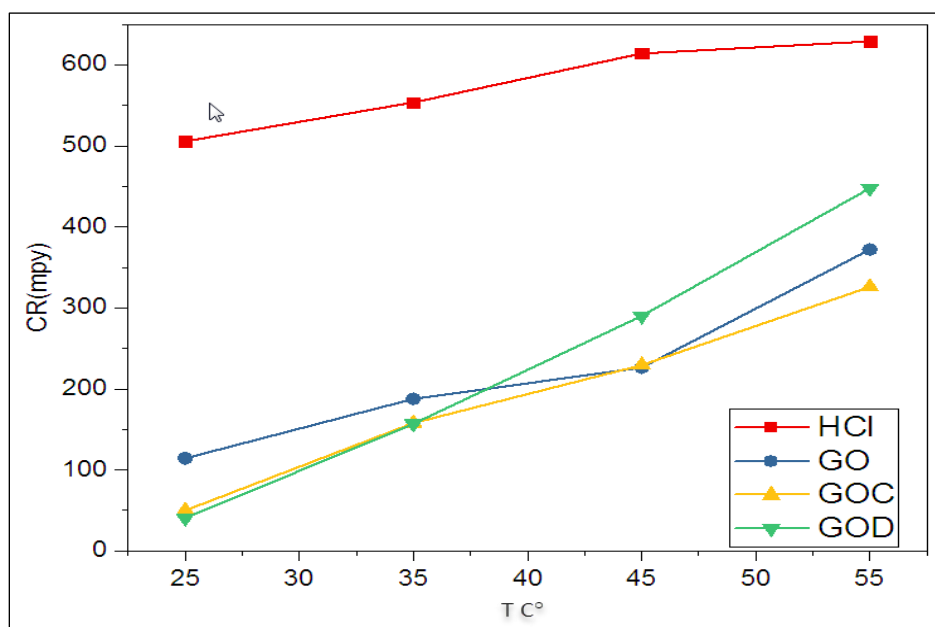


**Figure 9.** Effect of temperature on the corrosion rate in the absence and presence of GO, GOC and GOD inhibitors.

**Table 7.** Effect of temperature on the corrosion rate in the absence and presence of GO, GOC and GOD inhibitors.

Comp.	Temp (°C)	$E_{corr}$ (mV)	$I_{corr}$ ( $\mu A \cdot cm^{-2}$ )	CR (mpy)	$\beta_a$ (mV)	$\beta_c$ (mV)	$R_p$ ( $\Omega \cdot cm^2$ )	% IE	$\theta$
HCl	25	-611	1092	505.54	214.94	-240.19	16.488	—	—
	35	-620	1196	553.53	249.49	-248.25	15.059	—	—
	45	-599	1327	614.18	231	-259.9	13.571	—	—
	55	-614	1359	629.03	242.06	-366.58	13.251	—	—

Comp.	Temp (°C)	$E_{\text{corr}}$ (mV)	$I_{\text{corr}}$ ( $\mu\text{A}\cdot\text{cm}^{-2}$ )	CR (mpy)	$\beta_a$ (mV)	$\beta_c$ (mV)	$R_p$ ( $\Omega\cdot\text{cm}^2$ )	% IE	$\theta$
GO	25	-603	246.7	114.24	443.65	-458.22	72.963	77.4	0.774
	35	-619	405.1	187.58	236.52	-437.9	44.436	66.1	0.661
	45	-631	488.4	226.16	293.22	-287.56	36.856	63.2	0.632
	55	-614	803.4	372.03	313.81	-423.78	22.405	40.9	0.409
GOC	25	-656	107.8	49.887	255.01	-509.18	167.09	90.2	0.902
	35	-615	341	157.87	411.48	-393.46	52.8	71.5	0.715
	45	-609	495.2	229.31	306.83	-346.72	33.277	62.7	0.627
	55	-613	704	325.98	440.4	-430.26	25.57	48.2	0.482
GOD	25	-638	87.35	40.446	214.84	-676.57	206.09	92	0.92
	35	-612	339	156.94	194.25	-416.98	53.111	71.7	0.717
	45	-604	626.3	290	391.23	-421.23	28.742	52.8	0.528
	55	-588	967	447.77	178.43	-249.03	18.616	28.8	0.288

### 3.6. Kinetics Studies of prepared inhibitors

The present study includes the calculation of thermodynamic parameters such as activation energy ( $E_a$ ), enthalpy of activation ( $\Delta H^*$ ), entropy of activation ( $\Delta S^*$ ) and Gibbs free energy of activation ( $\Delta G^*$ ). To calculate and study the effect of temperature on  $E_a$  values at an optimal concentration in the absence and presence of the inhibitor, the Arrhenius equation for the rate can be used:

$$CR = A \exp\left[-\frac{E_a}{RT}\right] \quad (1)$$

Where CR is corrosion rate,  $A$  is the Arrhenius pre-exponential constant,  $E_a$  is the activation energy of the corrosion process,  $T$  is the absolute temperature (K) and  $R$  is the universal gas constant ( $8.3143 \text{ J}\cdot\text{K}^{-1}\cdot\text{mol}^{-1}$ ).  $E_a$  can be obtained from the slope of the plot of  $\ln CR$  versus  $1/T$  as shown in Figure 10 below, where the slope is equal to  $(-E_a/R)$  from Eq. (1). Notice that  $E_a$  values at optimal concentration in different temperatures of the prepared inhibitors were determined by linear regression between  $\ln CR$  versus  $1/T$ . Note that the  $E_a$  values in presence of the prepared inhibitors were higher than in their absence, which means that the corrosion reaction of carbon steel alloy in the absence inhibitors is very fast, while the presence of an inhibitor will make  $E_a$  higher. The range of  $E_a$  values of the inhibitors (from 6.29 kJ/mol to 76.32 kJ/mol) is lower than the threshold value of 80 kJ/mol required for chemisorption. It is thus concluded that physical adsorption of the inhibitors occurs. This increase in  $E_a$  values in the presence of inhibitors is attributed to an appreciable decrease in the adsorption process of the inhibitors on the alloy surface with

increasing temperature. The corresponding increase in the corrosion rate is also attributed to the greater area of the metal exposed to the corrosive environment, namely, the acid solution [12, 34–38].

The other thermodynamic parameters ( $\Delta H^*$  and  $\Delta S^*$ ) can be calculated from an alternative formulation of the Arrhenius equation:

$$\ln \frac{CR}{T} = \frac{RT}{Nh} \ln \left( \frac{\Delta S^*}{R} \right) - \left( \frac{\Delta H^*}{RT} \right) \quad (2)$$

Where CR is the corrosion rate,  $N$  is Avogadro's number ( $6.022 \times 10^{23} \text{ mol}^{-1}$ ),  $T$  is the absolute temperature (K),  $h$  is Plank's constant ( $6.62 \times 10^{-34} \text{ J}\cdot\text{s}$ ),  $\Delta H^*$  is the enthalpy of activation,  $\Delta S^*$  is the entropy of activation and  $R$  is the universal gas constant.  $\Delta H^*$  and  $\Delta S^*$  values can be obtained from the slope and intercept of the plot of  $\ln CR/T$  versus  $1/T$  as shown in Figure 11 below where the slope is equal to  $(-\Delta H^*/R)$  and the intercept is equal to  $(\ln R/Nh + \Delta S^*/R)$  from Eq. (2). The data shown in Table 8 and Figure 11 below revealed that  $\Delta H^*$  and  $\Delta S^*$  values for the dissolution reaction of the alloy in the presence of inhibitors were higher than in their absence. The positive sign of  $\Delta H^*$  refers to the endothermic nature of the dissolution process which implies that the dissolution of steel is difficult in the presence of inhibitors. On the other hand, the negative values of  $\Delta S^*$  show that the activated complex in the rate determining step represents an association rather than a dissociation step, meaning that a decrease in disorder take place on passage from the reactants to the activated complex. This behavior may be explained as a result of the replacement process of water molecules through adsorption of GO derivatives on the alloy surface. Furthermore, the  $\Delta G^*$  values were calculated by the following equation:

$$\Delta G^* = \Delta H^* - T\Delta S^* \quad (3)$$

Where  $\Delta G^*$  is the free energy of activation,  $\Delta H^*$  is the enthalpy,  $\Delta S^*$  is the entropy and  $T$  is the absolute temperature (K).  $\Delta G^*$  values were obtained from Eq. (3) at different temperatures as shown in Table 8, which implies that the  $\Delta G^*$  values in the presence of an inhibitor were higher than in its absence. Moreover, the  $\Delta G^*$  values were positive in the presence and in the absence of an inhibitor, which means that the corrosion process of the alloy is non-spontaneous [39, 40].

**Table 8.** Kinetic parameters for optimum concentrations in the absence and in the presence of inhibitors.

Comp.	Optimum Conc. (ppm)	$E_a$ ( $\text{kJ}\cdot\text{mol}^{-1}$ )	$\Delta H^*$ ( $\text{kJ}\cdot\text{mol}^{-1}$ )	$\Delta S^*$ ( $\text{J}\cdot\text{K}^{-1}\cdot\text{mol}^{-1}$ )	$\Delta G^*$ ( $\text{kJ}\cdot\text{mol}^{-1}$ )			
					298 K	308 K	318 K	328 K
HCl	0	6.29	3.62	-180.95	57.55	59.36	61.17	62.98
GO	70	30.30	28.22	-112.18	61.65	62.78	63.90	65.01
GOC	50	49.23	46.61	-54.26	62.78	63.33	63.87	64.41
GOD	70	76.30	61.49	-5.96	63.27	63.33	63.39	63.45

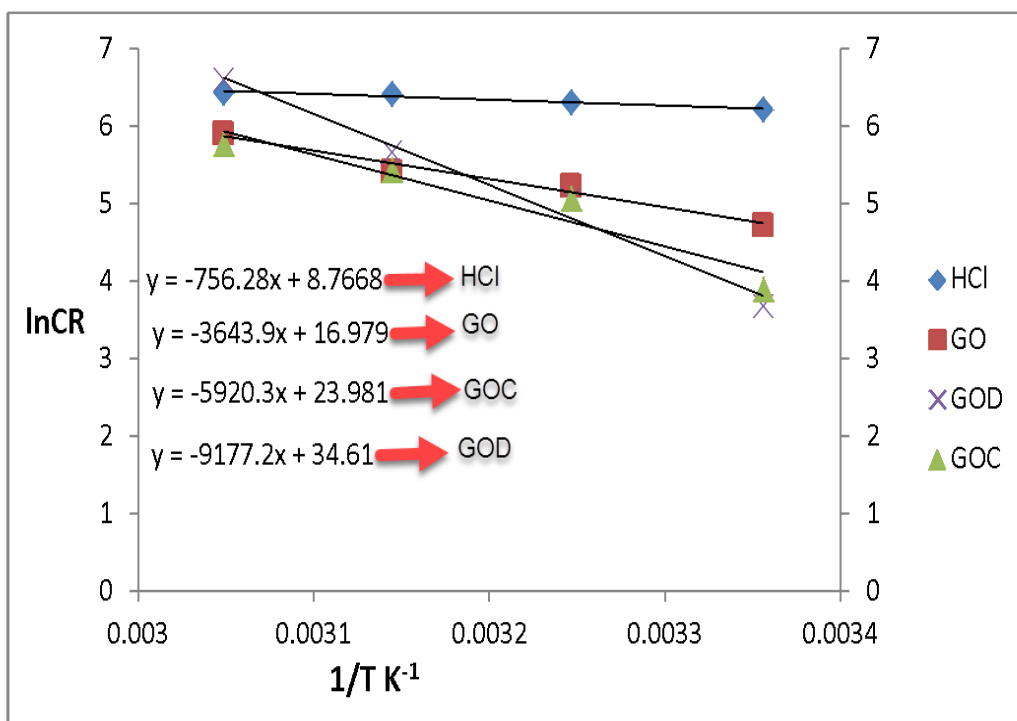


**Figure 10.** Calculation of the activation of energy in the absence and presence of GO, GOC and GOD inhibitors.

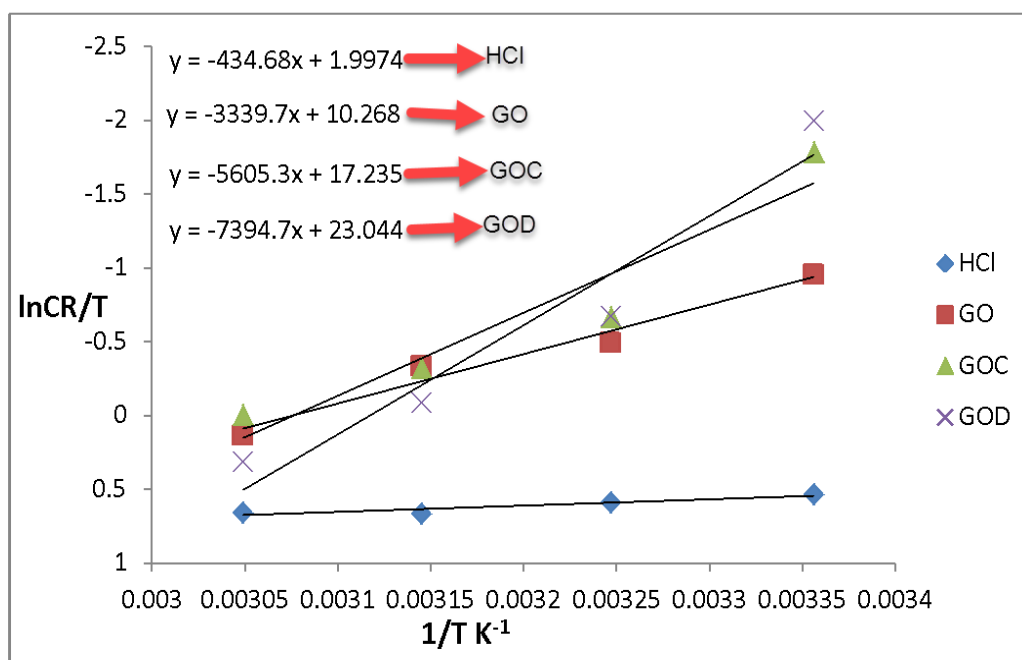


**Figure 11.** Calculation of  $\Delta H^*$  and  $\Delta S^*$  in the presence and absence of GO, GOC and GOD inhibitors.

### 3.7. Adsorption isotherm

An adsorption isotherm describes the adsorption process of a corrosion inhibitor that is very important as it gives information on the nature of interaction between a metal surface of an alloy and an inhibitor molecule. The adsorption of organic compounds at a metal/solution interface is due to either formation of electrostatic forces or formation of covalent bonding between the electrons of a heterocyclic inhibitor and the vacant orbitals of the metal surface. The Langmuir isotherm was used to describe the adsorption process of the prepared inhibitors GO, GOC and GOD. The most fitting isotherm of GO derivatives should give correlation coefficient values ( $R^2$ ) close to one, as shown in Figure 12 below, based on the following equation:

$$\frac{C_{\text{inhib}}}{\theta} = \frac{1}{K} + C_{\text{inhib}} \quad (4)$$

Where  $\theta$  is the surface coverage at optimal concentrations that can be calculated from Equation 5 below, where  $CR_{\text{unhib}}$  and  $CR_{\text{inhib}}$  are corrosion rates in the absence and presence of an inhibitor respectively at optimal concentrations and  $\theta$  values listed in Table 9,  $C$  is the concentration of the inhibitor in ppm and  $K$  is the equilibrium constant determined from the intercept of the Langmuir isotherm plot Eq. (5) between  $C/\theta$  inverse that presents linear behavior of the prepared inhibitors studied as shown in Figure 12 [31, 37].

$$\theta = \frac{CR_{\text{unhib}} - CR_{\text{inhib}}}{CR_{\text{unhib}}} \quad (5)$$

However there is a relationship between the equilibrium constant ( $K$ ) with the standard free energy of adsorption ( $\Delta G_{\text{ads}}^0$ ), as shown in the equation below:

$$\Delta G_{\text{ads}}^0 = -RT \ln(55.5)K_{\text{ads}} \quad (6)$$

where  $R$  is the universal gas constant,  $T$  is absolute temperature (K),  $K$  is the equilibrium constant,  $\Delta G_{\text{ads}}^0$  is the free energy of adsorption and 55.5 is the constant equal to the molar concentration of water in solution. Furthermore, from the Gibbs–Helmholtz Equation 7, one can calculate yet another thermodynamic function of the adsorption of prepared inhibitors at optimal concentration for different temperatures, namely  $\Delta H_{\text{ads}}^0$ .

$$\frac{\Delta G_{\text{ads}}^0}{T} = \frac{\Delta H_{\text{ads}}^0}{T} + k \quad (7)$$

Where  $\Delta H_{\text{ads}}^0$  is the standard adsorption enthalpy. The variation of  $\frac{\Delta G_{\text{ads}}^0}{T}$  versus  $\frac{1}{T}$  gives a straight line; according to Eq. (7), the slope of the plot is equal to  $\Delta H_{\text{ads}}^0$ , as Figure 13 shows. The standard adsorption entropy  $\Delta S_{\text{ads}}^0$  can be calculated from Eq. (8) [41]. The values of the thermodynamic parameters of the prepared inhibitors are shown in Table 10.

**Table 9.** Langmuir adsorption of prepared compounds at 298 K.

Comp.	Conc. ( ppm)	$\theta$	$C/\theta$	$R^2$
GO	10	0.623	16.06	0.9872
	30	0.642	46.73	
	50	0.639	78.25	
	70	0.717	97.63	
	100	0.774	129.2	
GOC	10	0.697	14.348	0.9924
	30	0.754	39.79	
	50	0.902	55.44	
	70	0.786	89.40	
	100	0.809	114.95	
GOD	10	0.802	12.47	0.9993
	30	0.875	34.29	
	50	0.879	56.89	
	70	0.92	76.09	
	100	0.90	111.11	

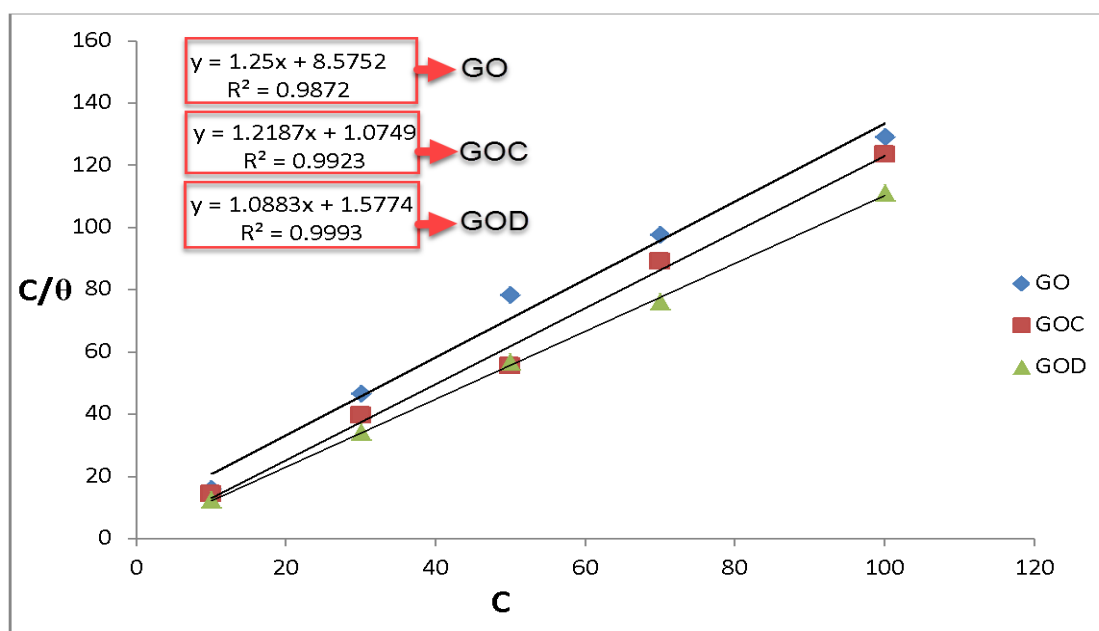


**Figure 12.** Langmuir adsorption isotherm plots of GO, GOC and GOD inhibitors.

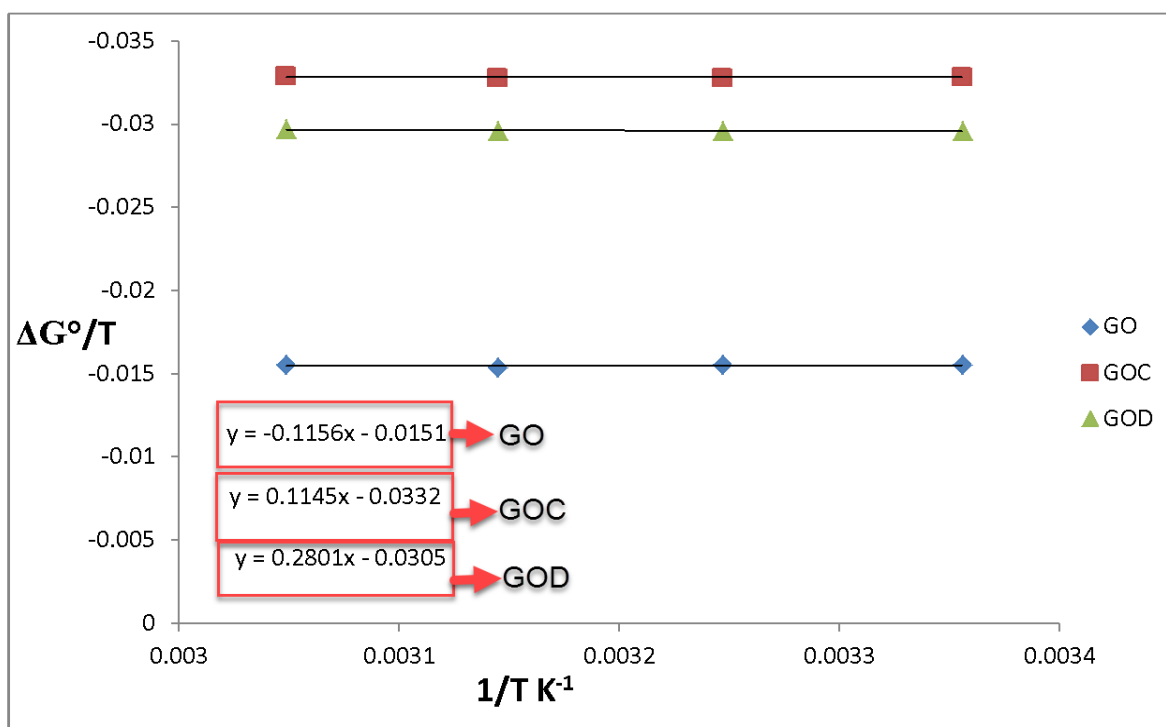


**Figure 13.** Calculation of  $\Delta H_{\text{ads}}^0$  for GO, GOC and GOD inhibitors.

**Table 10.** Thermodynamic parameters for prepared compounds.

Comp.	Temperature K	$\Delta G^0$ (kJ/mol·K)	$\Delta H^0$ (kJ/mol·K)	$\Delta S^0$ (J/mol·K)
GO	298	-4.63	-0.116	15.15
	308	-4.79		
	318	-4.94		
	328	-5.1		
GOC	298	-9.8	0.115	33.3
	308	-10.1		
	318	-10.43		
	328	-10.8		
GOD	298	-8.83	0.280	30.6
	308	-9.12		
	318	-9.42		
	328	-9.75		

$$\Delta S_{\text{ads}}^0 = \frac{\Delta H_{\text{ads}}^0 - \Delta G_{\text{ads}}^0}{T} \quad (8)$$

Table 10 shows that the  $\Delta G_{\text{ads}}^0$  values of the prepared inhibitors were negative, which indicates that the adsorption process of the compounds is spontaneous, where the negative sign refers to the stability of the adsorbed layer on the alloy surface. On the other hand, the  $\Delta G_{\text{ads}}^0$  values of the compounds prepared in this study increase with increasing temperature, that is, the values become less negative that lead to exothermic adsorption process. Generally when  $\Delta G_{\text{ads}}^0$  values are less than  $-20$  kJ/mol, this shows that the compounds prepared in this study are physically adsorbed [40, 42]. On the other hand, the  $\Delta H_{\text{ads}}^0$  values of the compounds have both positive and negative values, where the  $\Delta H_{\text{ads}}^0$  values for GOC and GOD were negative while the  $\Delta H_{\text{ads}}^0$  value of GO was positive. Negative  $\Delta H_{\text{ads}}^0$  values imply that adsorption of inhibitors is an exothermic process. Generally exothermic adsorption suggests either physical type or chemical type adsorption, while an endothermic process is attributed to chemical type adsorption. In an exothermic process, physical is compared to chemical type by considering the absolute  $\Delta H_{\text{ads}}^0$  value generally,  $\Delta H_{\text{ads}}^0$  value up to 41.86 kJ/mol is related to electrostatic interactions between charged molecules and charged metal surface (physical type) while a  $\Delta H_{\text{ads}}^0$  value around 100 kJ/mol or higher is attributed to chemical type. This means that negative  $\Delta H_{\text{ads}}^0$  values are physical type adsorption because  $\Delta H_{\text{ads}}^0$  values are up to 41.86 kJ/mol. While positive  $\Delta H_{\text{ads}}^0$  value of inhibitors (GOC and GOD) were very little, these compounds can be adsorbed by a simple endothermic process, indicating physical adsorption but its centers are chemically adsorbed. On the other hand,  $\Delta S_{\text{ads}}^0$  values of the prepared compounds are large and positive, this means that an increase in disordering on going from a reactant to the metal adsorbed reaction complex [37, 41].

#### 4. Conclusions

The prepared inhibitors are good inhibitors for carbon steel alloy in acid environment (0.1 M HCl) with inhibition efficiencies of 77.4%, 90.2% and 92% at optimum concentration of 100 ppm, 50 ppm and 70 ppm for GO, GOC and GOD, respectively. This indicates that the inhibition efficiency increases at optimum inhibitor concentration. Polarization curves (Tafel plots) demonstrate that the prepared compounds behave as mixed type inhibitors. The inhibition efficiency decreases with increasing temperatures, which implies that the prepared inhibitors are of physical adsorption type. Potentiodynamic measurements indicate that both the corrosion current density and corrosion rate values significantly decrease in the presence of the inhibitors compared with its absence. The prepared compounds inhibit by inhibitor adsorption on the alloy surface, simply blocking

the active sites. The adsorption of the compounds on the carbon steel alloy surface obeys the Langmuir adsorption isotherm since the  $R^2$  value is close to (1) between 10–100 ppm concentration. The free energy ( $\Delta G_{\text{ads}}^0$ ) of adsorption is negative, which indicates that the process is spontaneous and physical adsorption on the steel surface occurs.

## References

1. S.R Nayak and K.N.S. Mohana, Corrosion protection performance of functionalized graphene oxide nanocomposite coating on mild steel, *Surf. Interfaces*, 2018, **11**, 63–73.
2. J. Liang *et al.*, Trilaminar structure hydrophobic graphene oxide decorated organosilane composite coatings for corrosion protection, *Surf. Coat. Technol.*, 2018, **339**, 65–77.
3. R. Ding *et al.*, A brief review of corrosion protective films and coatings based on graphene and graphene oxide, *J. Alloys Compd.*, 2018, **764**, 1039–1055.
4. P. Gupta and R.N. Goyal, Amino functionalized graphene oxide and polymer nanocomposite based electrochemical platform for sensitive assay of anti-doping drug atenolol in biological fluids, *J. Electrochem. Soc.*, 2016, **163**, no. 13, B601–B608.
5. N. Baig *et al.*, Diethylenetriamine functionalized graphene oxide as a novel corrosion inhibitor for mild steel in hydrochloric acid solutions, *New J. Chem.*, 2019, **43**, no. 5, 2328–2337.
6. A. Khalafi-Nezhad, B. Mokhtari and M.N.S. Rad, Direct preparation of primary amides from carboxylic acids and urea using imidazole under microwave irradiation, *Tetrahedron Lett.*, 2003, **44**, no. 39, 7325–7328.
7. A. Patel, V. Panchal and N. Shah, Electrochemical impedance study on the corrosion of Al-Pure in hydrochloric acid solution using Schiff bases, *Bull. Mater. Sci.*, 2012, **35**, no. 2, 283–290.
8. J. Yang *et al.*, Corrosion protection of iron in water by activated carbon fiber (ACF), *Carbon*, 2006, **44**, no. 1, 19–26.
9. K. Haruna *et al.*, Cyclodextrin-based functionalized graphene oxide as an effective corrosion inhibitor for carbon steel in acidic environment, *Progr. Org. Coat.*, 2019, **128**, 157–167.
10. O. Benali, O. Cherkaoui and A. Lallam, Adsorption and corrosion inhibition of new synthesized Pyridazinium-Based Ionic Liquid on Carbon steel in 0.5 M  $\text{H}_2\text{SO}_4$ , *J. Mater. Environ. Sci.*, 2015, **6**, 598–606.
11. A. Singh, A.K. Singh and M. Quraishi, Dapsone: a novel corrosion inhibitor for mild steel in acid media, *Open Electrochem. J.*, 2010, **2**, no. 1, 43–51.
12. L.A. Al Juhaiman, Polyvinyl pyrrolidone as a corrosion inhibitor for carbon steel in HCl, *Int. J. Electrochem. Sci.*, 2016, **11**, no. 3, 2247–2262.
13. B. Rani and B.B.J. Basu, Green inhibitors for corrosion protection of metals and alloys: an overview, *Int. J. Corros.*, 2012, **2012**.

14. L. Shahriary and A.A. Athawale, Graphene oxide synthesized by using modified hummers approach, *Int. J. Renew. Energy Environ. Eng.*, 2014, **2**, no. 1, 58–63.
15. C.-W. Lo, D. Zhu and H. Jiang, An infrared-light responsive graphene-oxide incorporated poly (N-isopropylacrylamide) hydrogel nanocomposite, *Soft Matter*, 2011, **7**, no. 12, 5604–5609.
16. C. Zhang *et al.*, Synthesis of amino-functionalized graphene as metal-free catalyst and exploration of the roles of various nitrogen states in oxygen reduction reaction, *Nano Energy*, 2013, **2**, no. 1, 88–97.
17. C. Caliman *et al.*, One-pot synthesis of amine-functionalized graphene oxide by microwave-assisted reactions: an outstanding alternative for supporting materials in supercapacitors, *RSC Adv.*, 2018, **8**, no. 11, 6136–6145.
18. K. Żelechowska *et al.*, Fully scalable one-pot method for the production of phosphonic graphene derivatives, *Beilstein J. Nanotechnol.*, 2017, **8**, no. 1, 1094–1103.
19. S. Kumari, A. Shekhar and D.D. Pathak, Synthesis and characterization of a Cu (II) Schiff base complex immobilized on graphene oxide and its catalytic application in the green synthesis of propargylamines, *RSC Adv.*, 2016, **6**, no. 19, 15340–15344.
20. B. Xue *et al.*, Facile functionalization of graphene oxide with ethylenediamine as a solid base catalyst for Knoevenagel condensation reaction, *Catal. Comm.*, 2015, **64**, 105–109.
21. A. Gupta, B.K. Shaw and S.K. Saha, Photoluminescence study of optically active diaminopyridine intercalated graphene oxide, *RSC Adv.*, 2014, **4**, no. 92, 50542–50548.
22. B. Paulchamy, G. Arthi, and B. Lignesh, A simple approach to stepwise synthesis of graphene oxide nanomaterial, *J. Nanomed. Nanotechnol.*, 2015, **6**, no. 1, 1.
23. Z. Mou *et al.*, Forming mechanism of nitrogen doped graphene prepared by thermal solid-state reaction of graphite oxide and urea, *Appl. Surf. Sci.*, 2011, **258**, no. 5, 1704–1710.
24. M.H.M. Zaid and J. Abdullah, Preparation and characterization of amine functionalized graphene oxide with water soluble quantum dots for sensing material, in *AIP Conference Proceedings*, 2017, AIP Publishing.
25. A.V. Nakhate and G.D. Yadav, Synthesis and characterization of sulfonated carbon-based graphene oxide monolith by solvothermal carbonization for esterification and unsymmetrical ether formation, *ACS Sustainable Chem. Eng.*, 2016, **4**, no. 4, 1963–1973.
26. H. Kharkwal, H. Joshi, and K. Singh, Fabrication and Characterization of Layered Graphene Oxide Biocompatible Nano-Film by Various Methods, *Int. J. Biochem. Biophys.*, 2018, **6**, no. 1, 1–19.
27. S. Rani, D. Kumar and M. Kumar, Improvement in humidity sensing of graphene oxide by amide functionalization, *Sens. Transducers*, 2015, **193**, no. 10, 100.
28. W.-C. Oh and F.-J. Zhang, Preparation and characterization of graphene oxide reduced from a mild chemical method, *Asian J. Chem.*, 2011, **23**, no. 2, 875.

- 
29. L. Lai *et al.*, One-step synthesis of NH<sub>2</sub>-graphene from in situ graphene-oxide reduction and its improved electrochemical properties, *Carbon*, 2011, **49**, no. 10, 3250–3257.
  30. M. Manssouri *et al.*, Adsorption proprieties and inhibition of mild steel corrosion in HCl solution by the essential oil from fruit of Moroccan *Ammodaucus leucotrichus*, *J. Mater. Environ. Sci.*, 2015, **6**, no. 3, 631–646.
  31. C. Loto and R. Loto, Effect of p-phenyldiamine on the corrosion of austenitic stainless steel type 304 in hydrochloric acid. Effect of P-Phenyldiamine on the Corrosion of Austenitic Stainless Steel Type 304 in Hydrochloric Acid, *Int. J. Electrochem. Sci.*, 2012, **7**, 9423–9440.
  32. H. Serrar *et al.*, Experimental and Theoretical Studies of the Corrosion Inhibition of 4-amino-2-(4-chlorophenyl)-8-(2,3-dimethoxyphenyl)-6-oxo-2,6-dihydropyrimido[2,1-b][1,3]thiazine-3,7-dicarbonitrile on Carbon Steel in a 1.0 M HCl Solution, *Port. Electrochim. Acta*, 2018, **36**, no. 1, 35–52.
  33. P. Okafor, V. Osabor and E. Ebenso, Eco-friendly corrosion inhibitors: inhibitive action of ethanol extracts of *Garcinia kola* for the corrosion of mild steel in H<sub>2</sub>SO<sub>4</sub> solutions, *Pigm. Resin Technol.*, 2007, **36**, no. 5, 299–305.
  34. J.I. Bhat and V. Alva, Corrosion inhibition of aluminium by 2-chloronicotinic acid in HCl medium, *Indian J. Chem. Technol.*, 2009, **16**, 228–233.
  35. M. Bahrami, S. Hosseini and P. Pilvar, Experimental and theoretical investigation of organic compounds as inhibitors for mild steel corrosion in sulfuric acid medium, *Corros. Sci.*, 2010, **52**, no. 9, 2793–2803.
  36. A.M.A. Al-Sammarraie and M.H. Raheema, Electrodeposited reduced graphene oxide films on stainless steel, copper, and aluminum for corrosion protection enhancement, *Int. J. Corros.*, 2017. **2017**.
  37. M. Lebrini, F. Robert and C. Roos, Adsorption properties and inhibition of C38 steel corrosion in hydrochloric solution by some indole derivates: temperature effect, activation energies, and thermodynamics of adsorption, *Int. J. Corros.*, 2013, **2013**.
  38. H.Z. Al-Sawaad, Synthesis, Characterization and Evaluation of 1,3-bis((2-aminopropyl)amino)methyl)-5-dimethylimidazolidine-2,4-dione (BAMMD) as corrosion inhibitor for carbon steel and brass alloys in 0.2 M NaCl, *Int. J. Adv. Res.*, 2015, **3**, no. 10, 343–361.
  39. M. Lebrini *et al.*, Corrosion inhibition by *Isertia coccinea* plant extract in hydrochloric acid solution, *Int. J. Electrochem. Sci.*, 2011, **6**, no. 7, 2443–2460.
  40. M. Dahmani *et al.*, Corrosion inhibition of C38 steel in 1 M HCl: A comparative study of black pepper extract and its isolated piperine, *Int. J. Electrochem. Sci.*, 2010, **5**, no. 8, 1060–1069.
  41. A. Ostovari *et al.*, Corrosion inhibition of mild steel in 1 M HCl solution by henna extract: A comparative study of the inhibition by henna and its constituents (Lawsone, Gallic acid,  $\alpha$ -d-Glucose and Tannic acid), *Corros. Sci.*, 2009, **51**, no. 9, 1935–1949.

- 
42. S. Ghareba and S. Omanovic, Interaction of 12-aminododecanoic acid with a carbon steel surface: towards the development of ‘green’ corrosion inhibitors, *Corros. Sci.*, 2010, **52**, no. 6, 2104–2113.

